

Numerical calculations of laminar and turbulent natural convection in water in rectangular channels heated and cooled isothermally on the opposing vertical walls

HIROYUKI OZOE, AKIRA MOURI and MASARU OHMURO

Department of Industrial and Mechanical Engineering, School of Engineering, Okayama University,
Okayama 700, Japan

STUART W. CHURCHILL

Department of Chemical Engineering, University of Pennsylvania,
Philadelphia, PA 19104, U.S.A.

NOAM LIOR

Department of Mechanical Engineering and Applied Mechanics, University of Pennsylvania,
Philadelphia, PA 19104, U.S.A.

(Received 25 December 1983)

Abstract—Natural convection was computed by finite-difference methods using a laminar model for 2×1 and 1×1 enclosures for Ra from 10^6 to 10^9 and $Pr = 5.12$ and 9.17 , and a k - ϵ turbulent model for a square enclosure for Ra from 10^{10} to 10^{11} and $Pr = 6.7$. The average Nusselt numbers agree well with the correlating equation of Churchill for experimental and computed values. The computed velocity profile along the heated wall is in reasonable agreement with prior experimental values except for the thin boundary layer along the lower part of the wall where a finer grid size than was computationally feasible appears to be necessary. A detailed sensitivity test for constants of the k - ϵ model was also carried out. The velocity profile at the middle height and the average Nusselt number was in even better agreement with the experimental results when the turbulent Prandtl number was increased to four and the constant c_1 was decreased by 10%. A more refined turbulent model and finer grid divisions appear to be desirable, particularly for larger Ra .

INTRODUCTION

TRANSITIONAL and turbulent convection in rectangular enclosures heated and cooled on two opposing vertical walls has a number of important applications, e.g. in the cases of a passive solar room heated by a Trombe wall and cooled by a north-facing window, and in the event of a breakdown of the circulating system in a nuclear reactor. This behavior has, however, received only limited attention because of its three-dimensionality, and the difficulty of numerically simulating the combination of boundary-layer-like flows near the heated and cooled walls and a slower gross circulation elsewhere.

Numerical solutions for the quasi-one-dimensional laminar, then transitional, and finally turbulent boundary layer along a vertical heated plate in an unconfined fluid have been carried out with the k - ϵ model for turbulence by Lin and Churchill [1], Plumb and Kennedy [2] and Farouk and Güçeri [3]. On the other hand, Fujii and Fujii [4] solved numerically for a turbulent boundary layer using the Glushko model. They carried out a detailed evaluation of their computed values and found qualitative agreement between the various turbulent characteristics and the available experimental data. Fraikin *et al.* [5] apparently obtained the first stable solution for

fundamentally two-dimensional turbulent natural convection. They studied a square channel with isothermally heated and cooled vertical walls and linear temperature profiles along the lower and upper horizontal boundaries. Their calculations were for air at Grashof numbers of 10^7 , 5×10^7 and 10^8 , which they postulated to be in the turbulent regime. Their maximum computed turbulent viscosity ranged from four times the molecular viscosity at $Gr = 10^7$ to 9.6 at 10^8 . They carried out a sensitivity analysis of the arbitrary coefficients in the k - ϵ model, but their results appear to be applicable only to their specific thermal boundary conditions. Farouk and Güçeri [6] used the k - ϵ model to compute laminar and turbulent natural convection in the horizontal concentric annulus between a heated inner and cooled outer cylinder at Rayleigh numbers up to 10^7 . They concluded that at higher Rayleigh numbers a finer grid would be necessary to simulate the thin boundary layers next to the walls.

Natural convection in finite rectangular enclosures is necessarily three-dimensional. The enclosures to be simulated in this work will, however, be assumed to be sufficiently deep (in the horizontal direction parallel to the heated and cooled walls) so that the time-averaged motion can be approximated as two-dimensional. Rayleigh numbers and Prandtl numbers for the

NOMENCLATURE

a_x, a_y, b_x, b_y	parameters in expression for grid location	Greek symbols	
$c_1, c_2, c_3, c_\mu, c_\epsilon$	parameters in k - ϵ model	α	thermal diffusivity [m ² /s]
E	dimensionless time-averaged rate of dissipation of turbulent energy = $\epsilon/(\alpha^3 Ra_L^{4/3}/L^4)$	α_t	eddy diffusivity for heat transfer [m ² /s]
g	acceleration due to gravity [m/s ²]	β	volumetric coefficient of expansion [K ⁻¹]
H	height of the cross-section of the enclosure	ϵ	time-averaged rate of dissipation of turbulent kinetic energy [m ² /s ³]
K	dimensionless time-averaged turbulent kinetic energy = $k/(\alpha Ra_L^{1/3}/L)^2$	ζ	dimensionless time-averaged vorticity = $(\partial V/\partial X) - (\partial U/\partial Y)$
k	turbulent kinetic energy = $(\overline{u^2} + \overline{v^2} + \overline{w^2})/2$ [m ² /s ²]	η	dummy variable
L	width of the enclosure [m]	θ	temperature [K]
l	scale of turbulence [m]	θ_0	= $(\theta_h + \theta_c)/2$ [K]
Nu	overall Nusselt number	κ	von Karman's constant ≈ 0.42
N_x	number of grid in X-direction	μ	viscosity [Pa·s]
N_y	number of grid in Y-direction	ν	kinematic viscosity = μ/ρ [m ² /s]
p	time-averaged pressure [Pa]	ν_t	eddy diffusivity [m ² /s]
Pr	Prandtl number = ν/α	ν_t^*	dimensionless time-averaged eddy diffusivity = $\nu_t/\alpha = c_\mu K^2/E$
Ra_L	Rayleigh number = $g\beta(\theta_h - \theta_c)L^3/(\alpha\nu)$	ξ	dummy variable
T	dimensionless time-averaged temperature	ρ	density [kg/m ³]
t	time [s]	σ	Prandtl number = ν/α
u	component of time-averaged velocity in x-direction [m/s]	σ_K	Prandtl number for the turbulent kinetic energy
U	dimensionless time-averaged velocity in x-direction = $Lu/(\alpha Ra_L^{1/3})$	σ_t	turbulent Prandtl number = ν_t/α
v	component of time-averaged velocity in y-direction [m/s]	σ_ϵ	Prandtl number for the rate of dissipation of turbulent energy
V	dimensionless time-averaged velocity in y-direction = $Lv/(\alpha Ra_L^{1/3})$	τ	dimensionless time = $Ra_L^{2/3}\alpha t/L^2$
X	dimensionless vertical coordinate = $xRa_L^{1/3}/L$	ψ	dimensionless time-averaged stream function.
x	vertical coordinate [m]		
Y	dimensionless horizontal coordinate = $yRa_L^{1/3}/L$	Subscripts	
y	horizontal coordinate [m].	0	dimensional reference value
		1, 2, 3	empirical constants of turbulent model
		c	center or central plane value
		H	height as a reference value
		h	heated wall
		L	width as a reference value
		l	cooled wall.

computations were chosen to match those of the available experimental data and thereby expedite comparisons.

TURBULENT MATHEMATICAL MODEL

The same two-dimensional k - ϵ model for turbulence

as employed by Fraikin *et al.* [5] and Farouk and Güçeri [6] was utilized in this investigation.

The following four equations represent in dimensionless form the conservation of the time-averaged vorticity, energy, turbulent kinetic energy and rate of dissipation of turbulent energy:

$$\frac{D\zeta}{D\tau} = (\sigma + \nu_t^*)\nabla^2\zeta + 2\left(\frac{\partial\nu_t^*}{\partial X}\frac{\partial\zeta}{\partial X} + \frac{\partial\nu_t^*}{\partial Y}\frac{\partial\zeta}{\partial Y}\right) - (\nabla^2\nu_t^*)\zeta + 2\left(\frac{\partial^2\nu_t^*}{\partial X^2}\frac{\partial V}{\partial X} - \frac{\partial^2\nu_t^*}{\partial Y^2}\frac{\partial U}{\partial Y} + 2\frac{\partial^2\nu_t^*}{\partial X\partial Y}\frac{\partial V}{\partial Y}\right) - \sigma\frac{\partial T}{\partial Y} \quad (1)$$

$$\frac{DT}{D\tau} = \left(1 + \frac{\nu_t^*}{\sigma_t}\right)\nabla^2 T + \frac{1}{\sigma_t}\left(\frac{\partial\nu_t^*}{\partial X}\frac{\partial T}{\partial X} + \frac{\partial\nu_t^*}{\partial Y}\frac{\partial T}{\partial Y}\right) \quad (2)$$

$$\begin{aligned} \frac{DK}{D\tau} = & \left(\sigma + \frac{v_t^*}{\sigma_K} \right) \nabla^2 K + \frac{1}{\sigma_K} \left(\frac{\partial v_t^*}{\partial X} \frac{\partial K}{\partial X} + \frac{\partial v_t^*}{\partial Y} \frac{\partial K}{\partial Y} \right) \\ & + v_t^* \left[\left(\frac{\partial U}{\partial Y} + \frac{\partial V}{\partial X} \right)^2 + 2 \left(\frac{\partial U}{\partial X} \right)^2 + 2 \left(\frac{\partial V}{\partial Y} \right)^2 \right] - E - \frac{\sigma}{\sigma_t} v_t^* \frac{\partial T}{\partial X} \end{aligned} \quad (3)$$

and

$$\begin{aligned} \frac{DE}{D\tau} = & \left(\sigma + \frac{v_t^*}{\sigma_\epsilon} \right) \nabla^2 E + \frac{1}{\sigma_\epsilon} \left(\frac{\partial v_t^*}{\partial X} \frac{\partial E}{\partial X} + \frac{\partial v_t^*}{\partial Y} \frac{\partial E}{\partial Y} \right) + C_1 \frac{E}{K} v_t^* \\ & \times \left[\left(\frac{\partial U}{\partial Y} + \frac{\partial V}{\partial X} \right)^2 + 2 \left(\frac{\partial U}{\partial X} \right)^2 + 2 \left(\frac{\partial V}{\partial Y} \right)^2 \right] - C_2 \frac{E^2}{K} - C_\epsilon \frac{\sigma}{\sigma_t} \frac{E}{K} v_t^* \frac{\partial T}{\partial X} \end{aligned} \quad (4)$$

Here the dimensionless time-averaged vorticity is defined as

$$\zeta = \frac{\partial V}{\partial X} - \frac{\partial U}{\partial Y} = -\nabla^2 \psi \quad (5)$$

and the dimensionless time-averaged stream function as

$$U = \frac{\partial \psi}{\partial Y}, \quad V = -\frac{\partial \psi}{\partial X} \quad (6)$$

The dimensionless time-averaged eddy diffusivity is related to the dimensionless time-averaged turbulent kinetic energy and the dimensionless time-averaged rate of dissipation of turbulent energy as follows:

$$v_t^* = c_\mu \frac{K^2}{E} \quad (7)$$

The following empirical constants recommended by Launder and Spalding [7] were used, except for c_ϵ in the buoyant term of the E -equation, which was adopted from Fraikin *et al.* [4]:

$$c_\mu = 0.09, \quad c_1 = 1.44, \quad c_2 = 1.92, \quad c_\epsilon = 0.7, \quad \sigma_K = 1, \quad \sigma_\epsilon = 1.3 \text{ and } \sigma_t = 1.$$

The dimensionless time-averaged variables in the above equations are defined as

$$X = \frac{x}{x_0}, \quad Y = \frac{y}{y_0}, \quad U = \frac{u}{u_0}, \quad V = \frac{v}{v_0},$$

$$\tau = \frac{t}{t_0}, \quad P = \frac{p}{p_0}, \quad K = \frac{k}{k_0},$$

$$E = \frac{\epsilon}{\epsilon_0}, \quad T = \frac{\theta - \theta_0}{\theta_h - \theta_l}, \quad v_t^* = \frac{v_t}{v_{t_0}},$$

$$x_0 = y_0 = \left[\frac{g\beta(\theta_h - \theta_l)}{\alpha\nu} \right]^{-1/3} = \frac{L}{Ra_L^{1/3}},$$

$$u_0 = v_0 = \frac{\alpha}{x_0} = \frac{\alpha}{L} Ra_L^{1/3},$$

$$p_0 = \rho \alpha^2 / x_0^2 = (\rho \alpha^2 / L^2) Ra_L^{2/3},$$

$$k_0 = \left(\frac{\alpha}{x_0} \right)^2 = \left(\frac{\alpha}{L} Ra_L^{1/3} \right)^2,$$

$$\epsilon_0 = \alpha^3 / x_0^4 = \alpha^3 Ra_L^{4/3} / L^4, \quad v_{t_0} = \alpha,$$

$$t_0 = \frac{x_0}{u_0} = L^2 / (Ra_L^{2/3} \alpha)$$

The system which was studied is sketched in Fig. 1. The following boundary conditions were used:

(1) Temperature

$$T = 0.5 \quad \text{at} \quad Y = 0 \quad (8)$$

$$T = -0.5 \quad \text{at} \quad Y = \left(\frac{L}{H} \right) Ra_H^{1/3} \quad (9)$$

(2) Velocity and stream function

$$\psi = U = V = 0 \quad \text{at} \quad \begin{cases} X = 0, Ra_H^{1/3} \\ Y = 0, (L/H)Ra_H^{1/3} \end{cases} \quad (10)$$

(3) Vorticity

$$\zeta = \frac{\partial V}{\partial X} = -\frac{\partial^2 \psi}{\partial X^2} \quad \text{at} \quad X = 0, Ra_H^{1/3} \quad (12)$$

$$\zeta = -\frac{\partial U}{\partial Y} = -\frac{\partial^2 \psi}{\partial Y^2} \quad \text{at} \quad Y = 0, Ra_H^{1/3}(L/H) \quad (13)$$

(4) Turbulent kinetic energy

$$K = 0 \quad \text{at} \quad \begin{cases} X = 0, Ra_H^{1/3} \\ Y = 0, (L/H)Ra_H^{1/3} \end{cases} \quad (14)$$

(5) Rate of dissipation of turbulent energy

The time-averaged rate of dissipation of turbulent energy, ϵ , is proportional to $k^{3/2}/l$ where l is a characteristic length expressing the scale of the turbulence. Since k and l both approach zero at the wall, the boundary condition for ϵ is undefined. However, ϵ is almost constant near the wall, and it follows from assuming the length scale to be proportional to the distance Δy from the wall that

$$\epsilon = \frac{c_\mu^{3/4} k^{3/2}}{\kappa \Delta y} \quad \text{at} \quad y = 0, L \quad (16)$$

or

$$E = \frac{c_\mu^{3/4} K^{3/2}}{\kappa \Delta Y} \quad \text{at} \quad Y = 0, Ra_H^{1/3}(L/H) \quad (17)$$

Here, κ = von Karman constant = 0.42

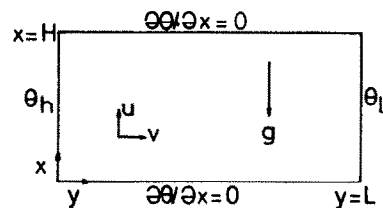


FIG. 1. Scheme of the system.

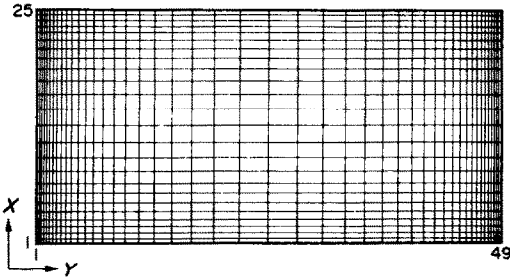


FIG. 2. Example of grid point distribution for $L/H = 2$.

Setting $\varepsilon = k = 0$ on the surfaces, as proposed by Jones and Launder [8], was also tried, with additional terms in the k and ε equations for a low Reynolds number. However k and ε then either converged to zero at all grid points or diverged.

GRID SIZE DISTRIBUTION

For the conditions of interest, a boundary layer flow, in which the velocity changes drastically, occurs near the surfaces, whereas the fluid is nearly stagnant in the central region. A fine grid-size is therefore preferable near the surfaces and a coarse one in the core. Accordingly, the X and Y locations of the grid were determined in terms of the equally divided dummy coordinates ξ and η as follows:

$$X = \frac{1}{a_x} (e^{\xi/b_x} - 1) \quad \text{for } 0 < \xi < \frac{Ra_H^{1/3}}{2} \quad (18)$$

$$X = \frac{1}{a_x} (1 + a_x - e^{\xi/b_x}) \quad \text{for } \frac{1}{2} Ra_H^{1/3} < \xi < Ra_H^{1/3} \quad (19)$$

$$Y = \frac{1}{a_y} (e^{\eta/b_y} - 1) \quad \text{for } 0 < \eta < \left(\frac{L}{2H}\right) Ra_H^{1/3} \quad (20)$$

and

$$Y = \frac{1}{a_y} (1 + a_y - e^{\eta/b_y}) \quad \text{for } \frac{L}{2H} (Ra_H^{1/3}) < \eta < \frac{L}{H} Ra_H^{1/3} \quad (21)$$

The resulting grid is illustrated in Fig. 2 for $L/H = 2$ with $N_x = 24$, $N_y = 48$, $a_x = 39.283$, $b_y = 0.16516$, $a_x = 5.8765$, $b_x = 0.36476$.

COMPUTED RESULTS FOR LAMINAR REGIME

Test calculations for the laminar regime were carried out for aspect ratios of $L/H = 1$ and 2 simply by setting $v_x^* = 0$ in equations (1) and (2) and dropping equations (3) and (4).

Case I: $L/H = 2$

This aspect ratio was chosen to simulate a large room. The first calculations were for $Pr = 9.17$ with the sudden imposition of a temperature difference equivalent to $Ra = 10^6$. The grid locations were calculated for the parametric values in the first line of Table 1.

The transient response of the overall Nusselt number and the central value of the dimensionless stream function are shown in Fig. 3. A rapidly damped oscillation about the steady state solution can be observed. Steady state velocity vectors and dimensionless isotherms are shown in Fig. 4 (a) and (b), respectively.

Computations were next carried out for $Ra = 10^7$ and $Pr = 9.17$ with the same grid. However, the maximum computed vertical velocity occurred on the grid line nearest the heated (and cooled) wall, suggesting that an even higher velocity might occur nearer the wall. Therefore, the number of divisions, N_x and N_y , were increased to 24 and 48, respectively, and the other grid-size parameters changed as indicated in the second line of Table 1. This gave the more reasonable solution illustrated in Fig. 5 by the velocity vectors, dimensionless temperatures, and streamlines. Boundary layers near the surfaces and stratification in the core are more firmly established than for $Ra = 10^6$.

Similar computations for $Ra = 10^8$ and $Pr = 9.17$ yielded a convergent solution with the dimensionless isotherms and streamlines shown in Fig. 6. The standing vortices and tortuous streamlines of Fig. 6 were not observed in the experimental work of Ozoe *et al.* [9] in a 160 mm high, 295 mm wide and 189 mm deep enclosure at the same Rayleigh and Prandtl numbers. The location of the center of the principal standing vortex was the same as that of the maximum value in the vertical velocity, suggesting that too large a vertical velocity in comparison to the grid size might have caused this unrealistic behavior. The maximum cell Reynolds number at this location was $U_{\max} \Delta X / Pr = 5.8(33.58)/9.17 = 21.2$ which is much higher than the

Table 1. Coefficients for the calculation of the grid locations

Ra	L/H	N_x	N_y	a_x	b_x	a_y	b_y
10^6	2	20	20	(Equal size in x-direction)		94.311	0.12905
$10^7, 1.52 \times 10^8$	2	24	48	5.8765	0.36476	39.283	0.16516
$10^6, 10^7$	1	24	24	5.8765	0.36476	39.283	0.16516
$10^8, 10^9$	1	24	48	16.699	0.22368	76.031	0.13646
10^{10}							
6.3×10^{10}	1	24	60	33.223	0.17430	94.787	0.12889
1.09×10^{11}							

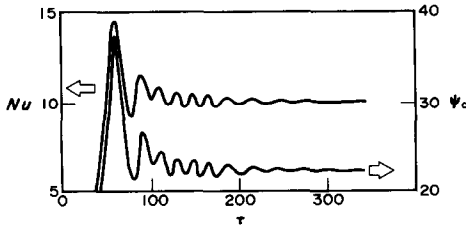


FIG. 3. Illustration of convergence of transient calculations for the Nusselt number and dimensionless central stream function for $Ra = 10^6$ and $Pr = 9.17$.

zero overshoot criterion of 2.0, suggested by Roache [10]. The value of 21.2 appears to be too large even for an implicit finite-difference formulation. One method of reducing the cell Reynolds number would be to use a smaller grid, but the resulting increase in computation would be prohibitive. Another remedy would be to use an upwind formulation. However, the simple upwind method has a first-order truncation error. Instead of either of these, the hybrid scheme suggested by Patankar [11] was utilized. This scheme employs the upwind method only when the coefficient matrix becomes negative due to a large value of the velocity in the convective term. All other points are approximated by central differences.

The computations with this hybrid scheme converged successfully for $Ra = 1.52 \times 10^8$ and $Pr = 9.17$, as illustrated in Fig. 7, producing the velocity vectors, dimensionless isotherms, and streamlines shown in Fig. 8.

Evaluation of computed result. The overall Nusselt for $L = 2H$ (rectangles) is compared with the correlating equation of Churchill [12] in Fig. 9. The agreement is good but the computed value falls slightly below the

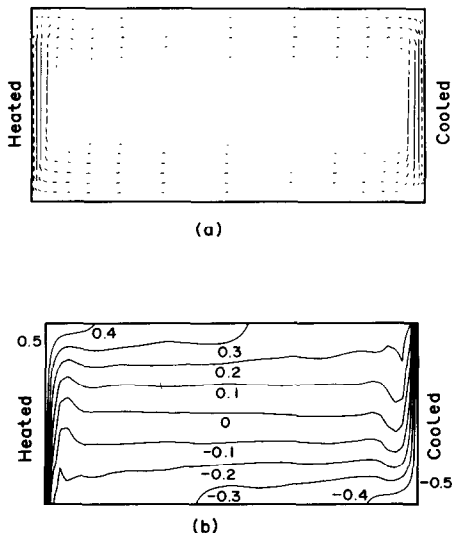


FIG. 4. Steady state solution for $Ra = 10^6$ and $Pr = 9.17$. (a) Velocity vectors; (b) dimensionless isotherms.

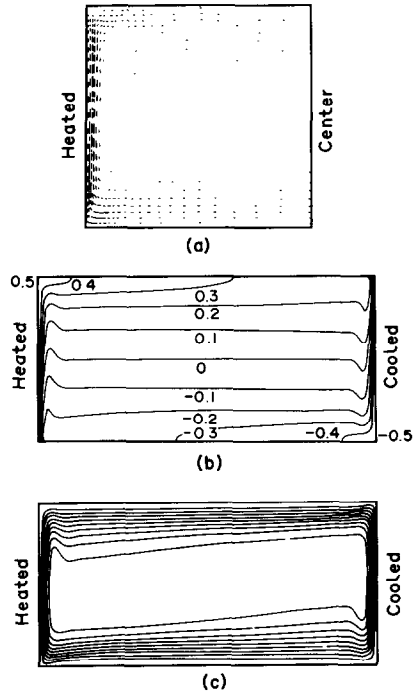


FIG. 5. Steady state solution for $Ra = 10^7$ and $Pr = 9.17$. (a) Velocity vectors; (b) dimensionless isotherms; (c) streamlines.

correlating equation, probably because the number of grid points is still insufficient. The mean Nusselt number predicted by the correlation of Churchill and Usagi [13] for a heated vertical plate in an unconfined fluid is also shown in Fig. 9. The deviation from that curve represents the effect of the horizontal surfaces, which for this aspect ratio is considerable.

The computed maximum vertical velocity near the

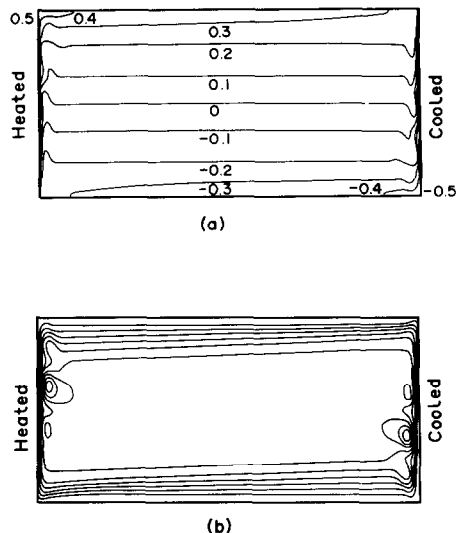


FIG. 6. Steady state solution for $Ra = 10^8$ and $Pr = 9.17$. (a) Dimensionless isotherms; (b) streamlines.

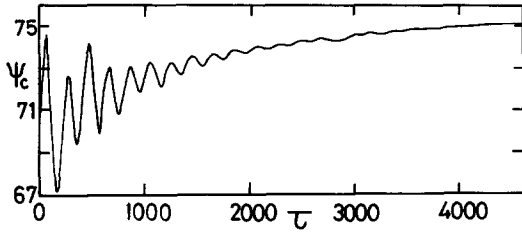


FIG. 7. Transient response of the dimensionless central stream function for $Ra = 1.52 \times 10^8$ and $Pr = 9.17$ with $\Delta\tau = 0.1$ to 0.2 .

heated wall can be represented by the empirical expression

$$U_{max} = 0.269 Ra_H^{0.162} \quad (22)$$

or

$$u_{max} = 0.269 \left(\frac{\alpha}{H}\right) Ra_H^{0.495} \quad (23)$$

Hishida and Tsuji [14] correlated the maximum vertical velocity along a heated vertical plate in unconfined air by

$$u_{max} = b \left(\frac{\alpha}{x}\right) Ra_x^{0.493} \quad (24)$$

with $b = 0.267$ for $Gr_x \geq 10^{10}$, and $b = 0.394$ for $Gr_x \leq 10^9$. The exponent of the Rayleigh number agrees remarkably well. The coefficient would not be expected to coincide, considering the difference in the boundary conditions, in Pr , and in the range of Ra .

Ozoe *et al.* [9] measured the vertical velocity in water at the mid-depth along the heated wall of a 160 mm high, 295 mm wide and 189 mm deep enclosure for a temperature difference corresponding to $Ra = 1.52 \times 10^8$ and $Pr = 9.17$. Their values are compared in Fig. 10 with those computed herein. The agreement is excellent with the values measured at the height of 75 mm, but is poor with those at 15 mm. These velocity profiles are not normalized with respect to the peak

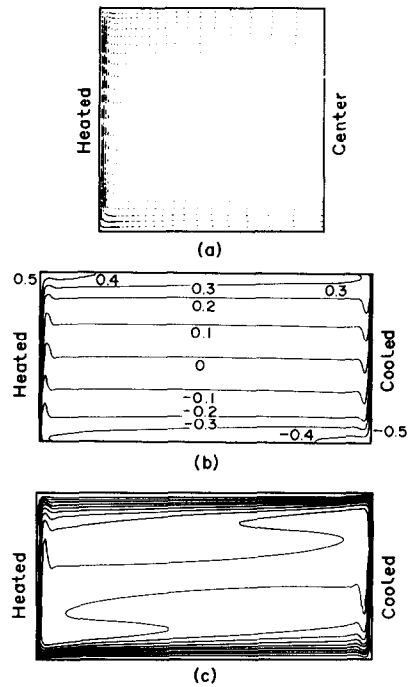


FIG. 8. Steady state solution for $Ra = 1.52 \times 10^8$ and $Pr = 9.17$ using the hybrid scheme of Patankar [11]. (a) Velocity vectors; (b) dimensionless isotherms; (c) streamlines.

value and the normalized y coordinate (which would reduce the effect of the finite depth in the experiments and the finite number of grid points in the computations), and thereby constitutes a critical test of the simulation. The corresponding peak velocities at various heights are compared in Fig. 11. The curve representing the computations is higher than the experimental values at low elevations, in good agreement at intermediate elevations and lower at high elevations.

It may be noted in Fig. 10 that only one grid point falls between the peak velocity and the wall at an

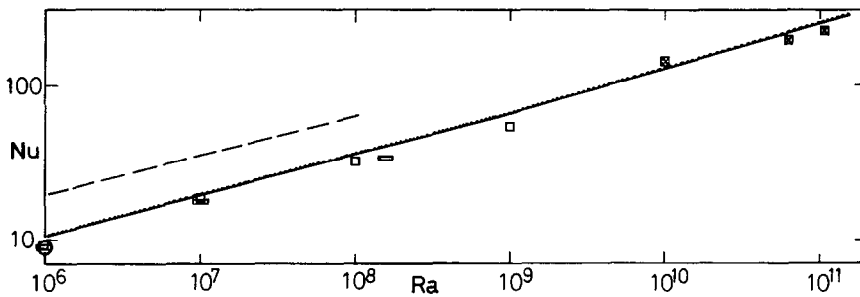


FIG. 9. Comparison of the computed overall Nusselt number with correlating equation of Churchill [12] for $L/H = 1$ and 2 .
 $L/H = 2$ □ Laminar model — Correlating equation
 $L/H = 1$ □ Laminar model ⊗ Turbulent model ---- Correlating equation
 ○ Comparison problem report [15]
 ---- Correlating equation for vertical plate in unconfined fluid [13].

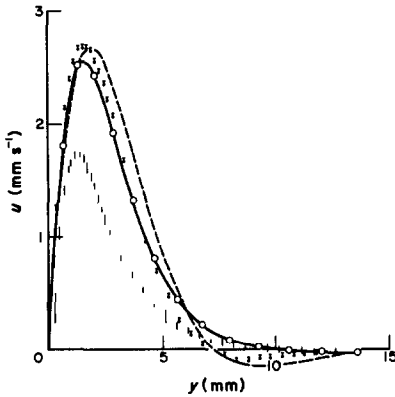


FIG. 10. Comparison for $Ra = 1.52 \times 10^8$ and $Pr = 9.17$ of the computed vertical velocities with experimental values in a 160 mm high, 295 mm wide and 189 mm deep enclosure.
 △ Measured vertical velocity at $x = 15$ mm
 ■ Measured vertical velocity at $x = 75$ mm
 -○- Computed vertical velocity at a height equivalent to $x = 15.8$ mm
 -- Computed vertical velocity at a height equivalent to $x = 80$ mm.

elevation corresponding to 15 mm. The peak velocity fell right on the first grid point at an elevation of 3.5 mm (not shown). Thus even 48 horizontal divisions are insufficient to provide reliable results at this level of detail.

Case II: $L/H = 1$

Computations were also carried out for the classical case of a square channel in order to relieve the grid-size requirement somewhat. These computations were for $Ra = 10^6, 10^7, 10^8, 10^9$ and $Pr = 5.12$. The grid size parameters are shown in lines 3 and 4 of Table 1. The computed overall Nusselt numbers are shown in Fig. 9 with square symbols. De Vahl Davis and Jones [15] reported a summary of competitive solutions for a square channel with the same boundary conditions as this work for $Ra = 10^4, 10^5$ and 10^6 . The best value of the average Nusselt number at $Ra = 10^6$ is asserted by them to be 8.903 ± 0.09 . The agreement of the computations herein with this value is excellent, and the maximum velocities for the square channel are well represented by equations (22) and (23).

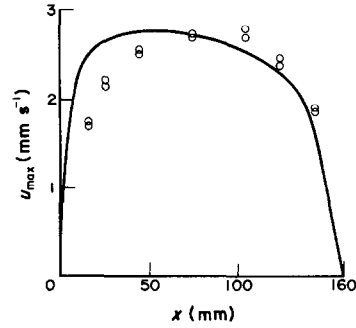


FIG. 11. Comparison of computed peak vertical velocities for $L/H = 2$, $Ra = 1.52 \times 10^8$ and $Pr = 9.17$ with experimental values.

— Computed
 ○ Range of fluctuation of experimental peak velocities in 160 mm high, 295 mm wide and 189 mm deep enclosure.

The computed velocity profiles for $Ra = 10^9$ are compared in Fig. 12 with the experimental measurements of Ozoe *et al.* [16] for water at $Ra = 1.04 \times 10^9$ and $Pr = 5.12$. The profiles are similar in shape but the experimental peak values are higher.

The computed values of the overall Nusselt number are tabulated in Table 2, together with some of turbulent results.

COMPUTED RESULTS FOR TURBULENT REGIME

The boundary layer along a vertical plate in an unconfined fluid is presumed to begin the transition to turbulent motion at $Gr = 10^9$ [12]. Turbulent motion of water in an enclosure heated on a vertical wall might therefore be expected to occur at $Ra = 10^9 Pr$. Accordingly, the $k-\epsilon$ model was evoked for $Ra \geq 10^{10}$.

Computations were successfully carried out for a square channel at $Ra = 10^{10}, 6.3 \times 10^{10}$ and 1.09×10^{11} with $Pr = 6.7$. The grid-distribution parameters are shown on line 5 of Table 1. The hybrid finite-difference scheme was again utilized.

All three cases yielded an oscillating but non-diverging solution as illustrated in Fig. 13 by the dimensionless, time-averaged central value of the stream function for $Ra = 6.3 \times 10^{10}$. The sinusoidal

Table 2. Summary of the computed cases plotted in Fig. 9

L/H	Ra	Pr	Nu	ψ_c	N_x	N_y	Model
1	10^6	9.17	9.38	20.4	24	24	laminar
1	10^7	9.17	18.8	33.5	24	48	laminar
1	10^8	5.12	31.7	56.0	24	48	laminar
1	10^9	5.12	53.5	104.1	24	48	laminar
1	10^{10}	5.12	146.1	*	24	60	$\sigma_1 = 1, c_1 = 1.44$
1	6.3×10^{10}	6.7	189	*	24	60	$\sigma_1 = 4, c_1 = 1.296$
1	1.09×10^{11}	6.7	213	*	24	60	$\sigma_1 = 4, c_1 = 1.296$
2	10^6	9.17	9.0	19.5	24	48	laminar
2	10^7	9.17	17.3	34.3	24	48	laminar
2	1.52×10^8	9.17	32.8	79.9	24	48	laminar

* Central value of the stream function oscillated.

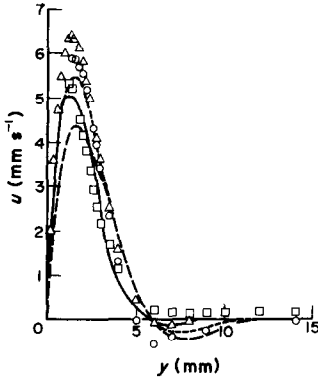


Fig. 12. Comparison of the vertical velocity near the heated vertical wall with experimental measurements in water by laser-Doppler velocimetry. Computed condition: $Ra = 10^9$, $Pr = 5.12$, $x = 43.2$ mm —, $x = 105$ mm - - -, $x = 166.8$ mm — — —. Experimental condition: $Ra = 1.04 \times 10^9$, $Pr = 5.12$, $x = 45$ mm \square , $x = 105$ mm \triangle , $x = 165$ mm \circ .

motion is presumed to correspond to real physical behavior. Staehle and Hahne [17], using a finite-difference method, computed transient oscillations, similar to those in Fig. 13, for rectangular channels heated and cooled on the opposing sides for a series of values of Ra less than 10^6 . They observed that the dampening of the oscillations decreased as the Rayleigh number increased, and therefore concluded that such oscillations would lead to turbulent motion at some higher value. Despite the oscillations in the time-averaged value of the central stream function, the time-averaged values of the velocity vector, the dimensionless temperature, and the stream function, which are plotted in Fig. 14 (a), (b) and (c), did not oscillate significantly near the walls. Apparently the slow, steady oscillation in the nearly stagnant core is effectively dampened in the relatively fast moving boundary layer near the surfaces. Contours of the dimensionless time-averaged turbulent kinetic energy, rate of dissipation of turbulent energy, and eddy diffusivity are plotted in Fig. 14 (d), (e) and (f). The maximum value of the eddy diffusivity ν_t^* is 93, which is about 14 times the Prandtl number. Thus the maximum eddy diffusivity is about 14 times the molecular kinematic viscosity.

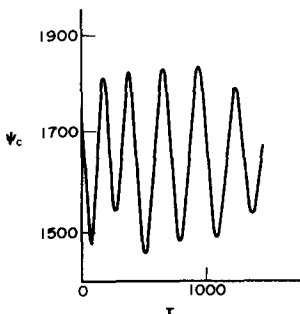


FIG. 13. Steady oscillations of the central stream function for $Ra = 6.3 \times 10^{10}$, $Pr = 6.7$ and $\Delta\tau = 1 \sim 3$.

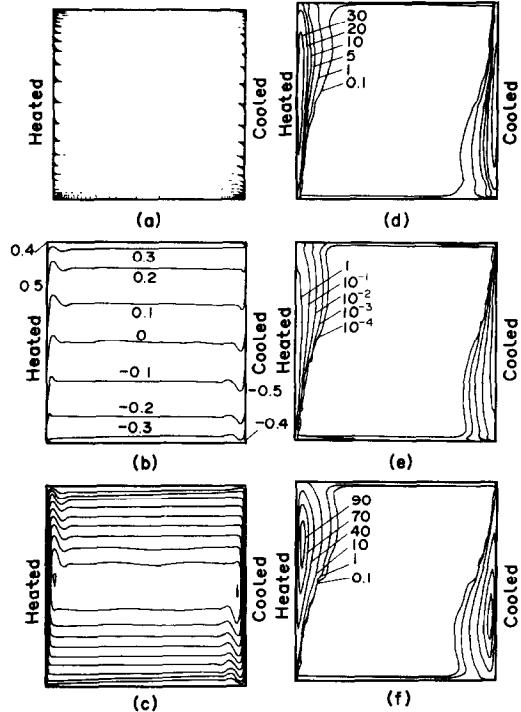


FIG. 14. Contour maps for the time-averaged characteristics of turbulent natural convection at $Ra = 6.3 \times 10^{10}$ and $Pr = 6.7$ in a square channel. (a) Velocity vectors; (b) dimensionless isotherms; (c) streamlines; (d) turbulent kinetic energy; (e) rate of dissipation of turbulent energy; (f) dimensionless eddy diffusivity.

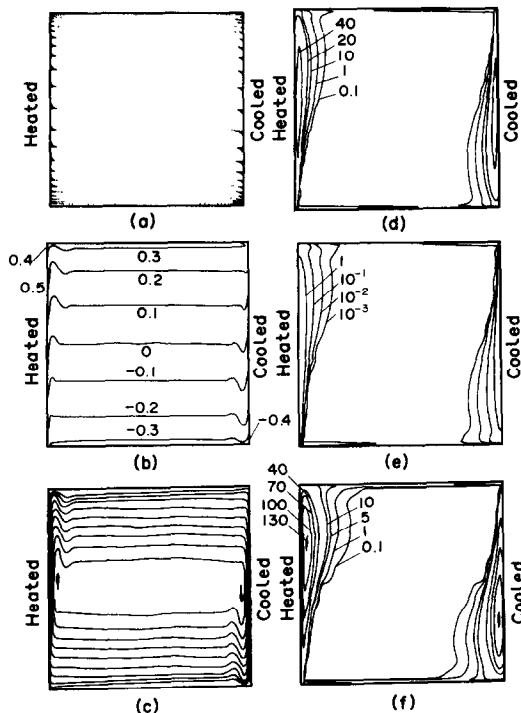


FIG. 15. Contour maps for the computed time-averaged characteristics of turbulent natural convection at $Ra = 1.09 \times 10^{11}$ and $Pr = 6.7$ in a square channel. (a) to (f) are the same as in Fig. 14.

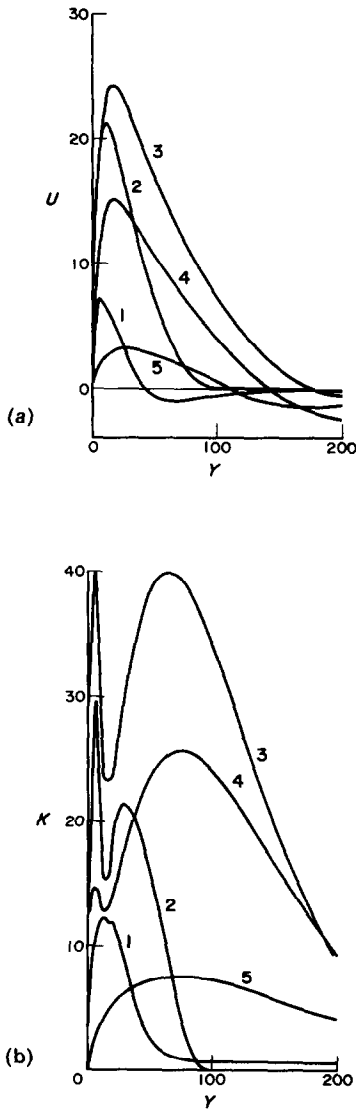


FIG. 16. Computed results for $Ra = 6.3 \times 10^{10}$ and $Pr = 6.7$ with standard set of constants in $k-\epsilon$ model. (a) Profiles of dimensionless vertical velocity at various heights; (b) profiles of dimensionless turbulent kinetic energy at various heights.

Curve	1	2	3	4	5
X	32.3	519	1990 (= $H/2$)	3460	3947

The same characteristics are plotted in Fig. 15 for $Ra = 1.09 \times 10^{11}$ and $Pr = 6.7$. Comparison with Fig. 14 indicates that the thickness of the boundary layer has increased with the Rayleigh number. However, a peak value near the bottom plate, as reported by Fraikin *et al.* [5], does not appear, probably because of the different boundary conditions.

A more detailed inspection of the computed result was made as follows. The dimensionless time-averaged vertical velocities at various heights were plotted in Fig. 16 (a) for $Ra = 6.3 \times 10^{10}$ and $Pr = 6.7$ vs the dimensionless normal distances from the surface.

Curves 1 to 5 represent the development and dampening of the vertical velocities from the bottom to the ceiling along the heated wall. Curve 1 at $X = 32.3$ corresponds to the first grid line from the bottom. The peak velocity is on the first grid from the vertical heated surface, suggesting a requirement of more grid points. The shape of the velocity profile of Curve 2 ($X = 519$) is similar to that of the laminar boundary layer, as seen in Fig. 10. The thickness of the boundary layer of curve 3 at $X = 1990$ (mid height) becomes more than double that of Curve 2. This appears to indicate a transition to turbulent flow. At higher levels, as seen in Curves 4 and 5, the upward flow dampens rapidly, with a downward velocity component outside the boundary layer flow.

In Fig. 16(b), the profiles of the dimensionless turbulent kinetic energy K are plotted vs the distance from the heated surface for the same heights as (a). The significant characteristic of these curves is the two-peak-profile. Hishida *et al.* [18] and Miyamoto *et al.* [19] measured $\overline{u'^2}/u^*$, where u^* is a friction velocity, for free convection of air along a heated vertical plate in an unconfined regime and reported a similar two-peak-profile. Fujii and Fujii [4] computed a similar two-peak-profile. This two-peak-profile of the turbulent kinetic energy appears to be one of the characteristics of turbulent free convection. A detailed observation of the variation of these profiles with height reveals that the first peak near the heated plate develops primarily due to the development of the strong upward velocity. The first peak is then dampened much more rapidly than the second peak because of the decreasing upward velocity against the top plate. The second peak occurs outside the peak of the vertical velocity of Fig. 16(a). This is due to the shear stress produced by the stagnant core of fluid at further distances from the wall.

The computed time-averaged values of the vertical velocity are compared in Fig. 17 with the experimental values of Ozoe *et al.* [16] for $Ra = 6.26 \times 10^{10}$, $Pr = 6.7$ and $x = 375$ mm (mid-height) for water in a 750 mm high, 750 mm wide and 180 mm deep enclosure. Curve 1 represents the vertical velocity profile at mid-height. The range of oscillation of the instantaneous experimental values is indicated by the vertical solid lines and their time-averaged values by the open circles. The computed values lie within the range of oscillation and have the same relative variation as the experimental ones. The computed values, however, are higher despite the expectation of agreement with the experimental time-averaged data as represented by the open circles. This disagreement might be caused by the arbitrary choice of some of the constants in the $k-\epsilon$ model. Therefore, a sensitivity test of these constants was carried out as follows.

Sensitivity test of the constants in the $k-\epsilon$ model

The standard combination of the constants was given above. Results for various perturbations are summarized in Table 3. This listing comprises the overall Nusselt number Nu , the maximum peak vertical velocity U_{\max} , the maximum value of the eddy

Table 3. Sensitivity test of constants in the k - ϵ model: $Ra = 6.3 \times 10^{10}$, $Pr = 6.7$, square channel

Condition	Nu	U_{\max}	$v_{t,\max}^*$	K_{\max}	E_{\max}	U at ($X = \text{mid height}$) ($Y = 76.14$)	Number of negative of K and E
Standard case	174.9	24.1	91.7	39.6	18.5	11.4	
$c_1 = 1.73 (+20\%)$	134.2	31.9	22.2	23.7	34.3	4.59	7
$c_1 = 1.152 (-20\%)$	210.8	21	154	39.8	12.3	11.1	3 in t.s.
$c_1 = 0.864 (-40\%)$	238.8	18.5	206	37.4	9.1	9.71	3 in t.s.
$c_2 = 2.304 (+20\%)$	212.7	22	164	42.8	14.4	12.1	3 in t.s.
$c_2 = 1.536 (-20\%)$	122	36.6	24.5	67.3	37.2		7
$c_1 = 1.152 (-20\%)$	241	19.4	210	39.6	10.5	10.5	
$c_2 = 2.304 (+20\%)$							
$c_1 = 1.584 (+10\%)$	214.4	22.4	167	43.9	15.3	12.5	2 in t.s.
$c_2 = 2.496 (+30\%)$							
$c_\epsilon = 1.44 (+106\%)$	176.6	24.6	100	39.9	68.3	11.6	35 negative in K 8 negative in E
$\sigma_\epsilon = 1.56 (+20\%)$	180	24.6	94.1	40.8	18.6	11.6	
$\sigma_K = 1.2 (+20\%)$	172	24.6	101	43.3	19.3	11.5	
$c_1 = 1.44$	153	34.4	139	77.9	46.4	21.3	6
$\sigma_1 = 0.5$							
$c_1 = 1.44$	185	20	55.3	27.7	9.8	5.0	
$\sigma_1 = 2$							
$c_1 = 1.44$	181	18.3	45.8	24.0	7.9	2.82	
$\sigma_1 = 3$							
$c_1 = 1.44$	176	17.5	39.5	25.2	7.00	1.92	
$\sigma_1 = 4$							
$c_1 = 1.44$	160	15.6	29.8	22.3	5.29	-0.33	
$\sigma_1 = 10$							
$c_1 = 1.152 (-20\%)$	219	17.0	103	32.2	7.29	6.04	
$\sigma_1 = 2$							
$c_1 = 1.152 (-20\%)$	208	16.1	87.1	29.9	6.43	4.59	
$\sigma_1 = 3$							
$c_1 = 1.152 (-20\%)$	181	14.2	61.1	27.5	5.17	1.68	
$\sigma_1 = 8$							
$\sigma_1 = 4$	189	16.5	58.4	28.1	6.54	2.95	
$c_1 = 1.296 (-10\%)$							
$\sigma_1 = 4$	212	14.6	98.2	30.0	5.72	3.88	
$c_1 = 1.008$							
$\sigma_1 = 4$	178	17.2	42.5	25.7	6.75	2.13	
$c_1 = 1.296$							
$c_2 = 1.776$							

diffusivity v_t^* , the maximum value of the turbulent kinetic energy K , the maximum value of the rate of dissipation of turbulent energy E and the vertical velocity at $Y = 76.14$, where the experimental vertical velocity becomes almost zero. Comparison with the experimental results may be described as follows.

The standard combination of the constants gives a slightly smaller Nusselt number than the correlation by Churchill [12] and too great a vertical velocity at middle height, as shown in Fig. 17.

Each constant was changed separately as much as $\pm 10\%$, $\pm 20\%$ or $\pm 30\%$ with the objective of obtaining better agreement of the velocity profile and the overall Nusselt number with experimental data.

Increasing the constant c_1 to 1.73 (+20%) gave too small a Nusselt number, and resulted in a much greater vertical velocity and a negative value of the turbulent kinetic energy K at seven grid points. The occurrence of a negative value of K is physically impossible, although the absolute value was within the computational error of order 10^{-10} to 10^{-15} , and can be considered to be an

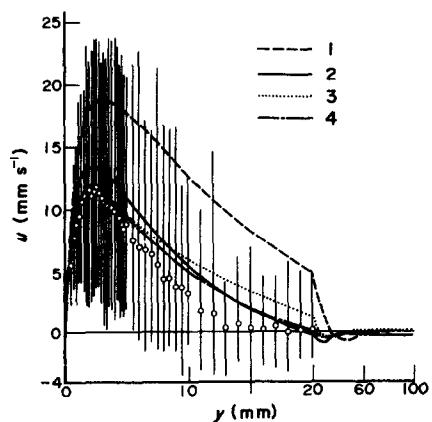


Fig. 17. Comparison of computed and experimental vertical velocities along the heated wall of a square enclosure for $Ra = 6.26 \times 10^{10}$, $Pr = 6.3$ and $x = 37.5$ cm. The experimental box is 750 mm \times 750 mm \times 180 mm.

Curve	1	2	3	4
σ_1	1	3	3	4
c_1	1.44	1.44	1.152 (-20%)	1.296 (-10%)

indication of an unrealistic combination of the constants in the model.

Decreasing the constant c_1 to 1.152 (−20%) gave a higher Nusselt number and a smaller peak velocity but the thickness of the boundary layer was observed to be unchanged. Decreasing c_1 by −40%, gave a similar effect, but more strongly.

Increasing c_2 by +20% produced almost the same effect as decreasing c_1 by 20%. Decreasing c_2 by 20% gave a negative value of the turbulent kinetic energy at seven grid points, and too small a value of the Nusselt number. Decreasing c_2 also resulted in a strange velocity profile and thereby is unacceptable.

A value of $c_2 = 1.44$ (+106%), which is equal to c_1 , was also tested. This resulted in 35 negative points in K and 8 negative points in E and hence was judged to be inappropriate. Apparently, the buoyant term in the E -equation must not be too large if negative values in K and E are to be avoided.

Increasing σ_v or σ_k by 20% did not change the mode of flow.

Finally the turbulent Prandtl number σ_t was changed to 0.5 (−50%). This resulted in negative values of the turbulent kinetic energy K at six grid points. On the other hand, $\sigma_t = 2$ (+100%) lowered the peak vertical velocity u_{max} from 24.1 to 20.

Figure 18 shows the effect of the change of the turbulent Prandtl number σ_t on the velocity and temperature profile at the middle height over the heated plate. Increasing σ_t from 0.5 to 10 resulted in a drastic decrease in the thickness of the velocity and thermal boundary layers. Let Y be the thickness of a boundary layer δ when the velocity becomes zero, and the thickness of a temperature boundary layer Δ when the temperature becomes zero. Such values are listed in Table 4. The ratio of these two thicknesses is almost the same, irrespective of the change of the turbulent Prandtl number. This characteristic is similar to that of laminar free convection for which the ratio of the thickness of the boundary layer is almost the same irrespective of the molecular Prandtl number.

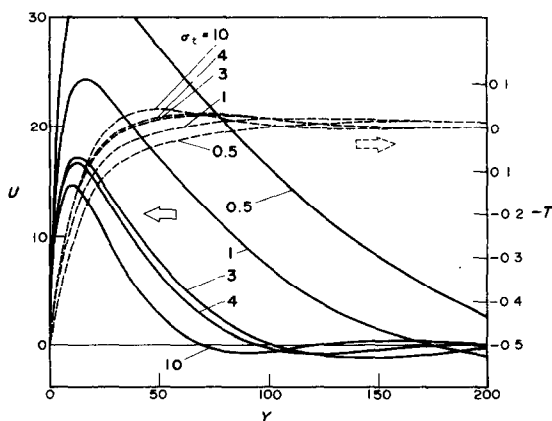


FIG. 18. Profiles of dimensionless vertical velocity and temperature at middle height for various values of the turbulent Prandtl number σ_t , $Ra = 6.3 \times 10^{10}$ and $Pr = 6.7$.

Table 4. Boundary layer thickness as effected by the turbulent Prandtl number σ_t . The value of Y when U and T first became zero was chosen as the boundary layer thicknesses δ and Δ , respectively: $Ra = 6.3 \times 10^{10}$, $Pr = 6.7$

σ_t	Y at $U = 0$ (δ)	Y at $T = 0$ (Δ)	Δ/δ
1	176	65	0.369
3	102	38.0	0.373
4	96.5	35.2	0.365
10	70.5	27.8	0.394

The ratio of the two thicknesses is unaffected by the turbulent Prandtl number.

Increasing σ_t above the unity appears to provide a better agreement of the computed vertical velocities with the experimental ones, probably due to the resulting thinner thermal boundary layer. This means that the temperature gradient near the heated wall becomes steeper. On the other hand, the maximum eddy diffusivity v_t^* decreases with increasing σ_t , and this should decrease the turbulent heat flux.

These two contradictory effects appear to give a slight increase of Nu at $\sigma_t = 2$ and then a decrease for greater values of σ_t . Constant c_1 was then simultaneously decreased so that both the velocity and the Nusselt number approach the experimental data. Setting c_1 to 1.152 (−20%) and $\sigma_t = 1, 2, 3$ and 8 was tested. The combination of $\sigma_t = 8$ and $c_1 = 1.152$ appears to give the best agreement of the Nusselt number and the thickness of the vertical velocity boundary layer, but too small a peak vertical velocity. Then, combined changes $\sigma_t = 4$ and $c_1 = 1.296$ (−10%) and $\sigma_t = 4$ and $c_1 = 1.008$ (−30%) were tried. The latter combination gave a little smaller peak velocity. According to Rodi [20], the constants c_1 and c_2 are related by

$$c_1 = c_2 - \frac{K^2}{\sigma_v \sqrt{c_\mu}} \quad (25)$$

This equation suggests that the change in c_1 from 1.44 to 1.296 should be accompanied by the same change in c_2 , i.e. $c_2 = 1.92 - 0.144 = 1.776$. The result of computations for this combination of the constants was found to be less effective and was not adopted. Some representative cases are plotted in Fig. 17 for the vertical velocity at mid-height. The combination of $\sigma_t = 4$ and $c_1 = 1.296$ appears to offer an appropriate compromise for the vertical velocity and the overall Nusselt number. The agreement is not completely satisfactory but is much better than with the standard combination of the constants as determined from forced convection.

Figure 19 shows a comparison of the temperature profile at mid-height with the experimental one. The combination of $\sigma_t = 4$ and $c_1 = 1.296$ (−10%) appears to give closer agreement with the experimental time-averaged values, as represented by open circles, than the standard set of constants.

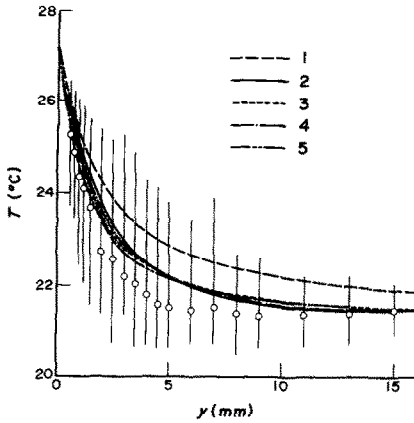


FIG. 19. Comparison of computed temperature profiles at mid-height for various combinations of constants in the $k-\epsilon$ model with the experimental measurements.

Curve	1	2	3	4	5
σ_t	1	3	3	4	4
c_1	1.44	1.44	1.152	1.296	1.008

The peak velocities at various heights are compared with the experimental ones in Fig. 20. Some representative combinations of constants of the turbulent Prandtl number σ_t and c_1 are plotted. The combination of $\sigma_t = 4$ and $c_1 = 1.296$ (-10%) again appears to give the best agreement with the experimental velocities. The overall Nusselt number for this combination is included in Fig. 9.

The profiles of the vertical velocity and the turbulent kinetic energy are shown in Fig. 21 (a) and (b) for $\sigma_t = 4$ and $c_1 = 1.296$. The peak velocity decreased 40% below that for the standard set of constants as used in Fig. 16(a). The two-peak profile of the turbulent kinetic energy, as seen in Fig. 16(b), is similar to the one for the standard set. However, the first peak does not develop

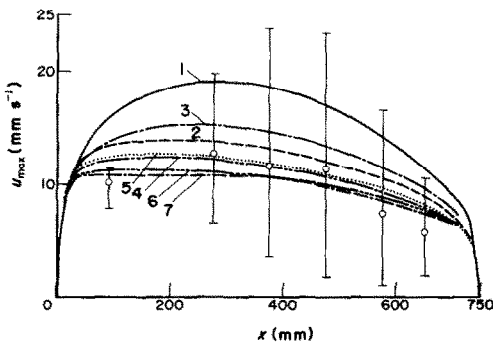


FIG. 20. Comparison for $Ra = 6.26 \times 10^{10}$ and $Pr = 5.12$ of the computed peak vertical velocities over the heated vertical wall of a square enclosure with the experimental oscillating velocities at the displacement corresponding to the peak velocity.

Curve	1	2	3	4	5	6	7
σ_t	1	3	2	3	4	4	8
c_1	1.44	1.44	1.156	1.156	1.296	1.008	1.156

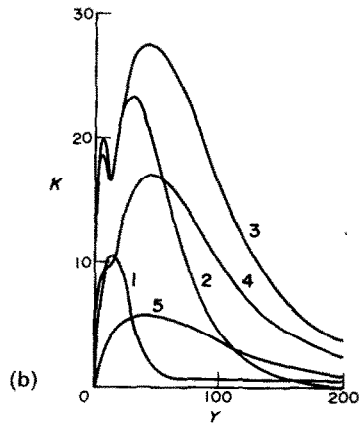
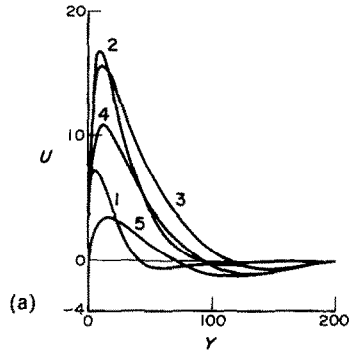


FIG. 21. Computed vertical velocity profiles, (a) and turbulent kinetic energy K_{10} (b) at various heights. $Ra = 6.3 \times 10^{10}$, $Pr = 6.7$, $\sigma_t = 4$ and $c_1 = 1.296$ (-10%).

Curve	1	2	3	4	5
X	32.3	519	1990	3460	3947

as much, probably due to lesser development of the vertical velocity.

The primary objective of this paper has been to develop a method of simulation for natural convection in an enclosure at high Rayleigh numbers. The total behavior of the convection in an enclosure can be simulated reasonably well with two-equation model, but the predictions of the detailed structure of the turbulent flow are difficult to assess because of the lack of available experimental data for the turbulent strength, eddy diffusivity, etc. The simulation of the details of boundary layer flows was studied by Plumb and Kennedy [2] using 40 to 80 grid points within the boundary layer and by Fujii and Fujii [4] using 200 grid points. When simulating the total behavior of convection within an enclosure some disagreement in the velocity and temperature profiles near the heated wall is unavoidable if only one or two grid points fall inside the boundary-layer-like flow. In the work reported herein the simplest model was employed for the buoyant term in ϵ -equation. The model proposed by Rodi [20] for a stratified flow might be useful with some modifications, but more detailed experimental data is essential to evaluate such alternative models.

SUMMARY AND CONCLUSIONS

1. Laminar natural convection in rectangular channels heated and cooled isothermally on the opposing vertical walls was successfully computed by a finite-difference method for Ra up to 10^9 with $Pr = 9.17$.

2. The accuracy of the calculations for laminar convection was improved by using the hybrid finite-difference scheme suggested by Patankar, with an upwind formulation replacing central differences only when necessary.

3. The overall Nusselt number for the laminar regime agreed well with the correlating equation of Churchill, and the peak velocity with the correlating equation of Hishida and Tsuji for a vertical plate in an unconfined fluid.

4. The computed velocity profile near the wall agreed well with the experimental measurements of Ozoe *et al.* at mid-height but was higher for low elevations and lower for high elevations. These deviations are undoubtedly due to an insufficient number of grid points within the boundary layer near the wall.

5. A two-dimensional k - ϵ model was used with a hybrid finite-difference scheme to compute turbulent natural convection in a square channel for Ra from 10^{10} to 10^{11} with $Pr = 6.7$.

6. A stable, slow, sinusoidal oscillation was computed for the central core in the turbulent regime. However the time-averaged velocity, temperature and turbulent characteristics were non-oscillatory within the boundary layers.

7. The computed time-averaged turbulent velocity profile near the heated wall fell within the range of oscillation of prior measured instantaneous velocities and agreed qualitatively with their time averages.

8. The computed overall Nusselt numbers for the turbulent regime are in reasonable agreement with the correlating equation of Churchill.

9. The constants of the two-equation model were changed separately and simultaneously to test their effect. The combination of a turbulent Prandtl number $\sigma_t = 4$ and a constant $c_1 = 1.296$ (-10%) gave a time-averaged vertical velocity profile, an overall Nusselt number, and a time-averaged temperature profile at mid-height in much better agreement with the experimental measurements than the standard set of constants for forced convection.

10. The effects of varying the constants in the k - ϵ model are complicated. Increasing the turbulent Prandtl number σ_t from unity decreases the peak value of the eddy diffusivity monotonically but the overall Nusselt number increases only up to $\sigma_t = 2$ and then decreases.

Acknowledgement—A part of this work was supported by the Grant in Aid for Scientific Research on Energy Problems sponsored by the Ministry of Education, Science and Culture, Japan. The valuable advice and comments offered by Dr. Hiroshi Kawamura of the Japan Atomic Energy Research Institute, are gratefully acknowledged. The computations were carried out on the Acos 700 and 1000 at the computer

center, Okayama University. The assistance of Mr. Masashi Hiramitsu, Okayama University is also acknowledged.

REFERENCES

1. S. J. Lin and S. W. Churchill, Turbulent free convection from a vertical isothermal plate, *Num. Heat Transfer* **1**, 129–145 (1978).
2. O. A. Plumb and L. A. Kennedy, Application of a k - ϵ turbulence model to natural convection from a vertical isothermal surface, *J. Heat Transfer* **99**, 79–85 (1977).
3. B. Farouk and S. I. Güçeri, Natural convection from a horizontal cylinder-turbulent regime, *J. Heat Transfer* **104**, 228–235 (1982).
4. M. Fujii and T. Fujii, Numerical calculation of turbulent free convection along a vertical plate, *Trans. JSME* **43**(374), 3825–3834 (1977) and **44**(384), 2797–2807 (1978).
5. M. P. Fraikin, J. J. Portier and C. J. Fraikin, Application of a k - ϵ turbulence model to an enclosed buoyance driven recirculating flow, 19th ASME-AIChE Nat. Heat Transfer Conference Paper, 80-HT-68, 1980.
6. B. Farouk and S. J. Güçeri, Laminar and turbulent natural convection in the annulus between horizontal concentric cylinder, *J. Heat Transfer* **104**, 631–636 (1982).
7. B. E. Launder and D. B. Spalding, The numerical computation of turbulent flows, *Comp. Meth. Appl. Mech. Eng.* **3**, 269–289 (1974).
8. W. P. Jones and B. E. Launder, The prediction of laminarization with a two-equation model of turbulence, *Int. J. Heat Mass Transfer* **15**, 301–314 (1972).
9. H. Ozoe, M. Ohmuro, A. Mouri, S. Mishima, M. Sayama and S. W. Churchill, Laser-Doppler measurements of the velocity along a heated vertical wall of a rectangular enclosure, *J. Heat Transfer* **105**, 782–788 (1983).
10. P. J. Roache, *Computational Fluid Dynamics*, Hermosa Publishers, Albuquerque, New Mexico (1972).
11. S. V. Patankar, *Studies in Convection*, Vol. 1, (edited by B. E. Launder), Academic Press, New York (1975).
12. S. W. Churchill, Free convection in layers and enclosures, Sec. 2.5.8, *Heat Exchanger Design Handbook*, (edited by E. U. Schlünder), Hemisphere Publishing, Washington, DC (1982).
13. S. W. Churchill and R. Usagi, A general expression for the correlation of rates of transfer and other phenomena, *AIChE J.* **18**, 1121–1128 (1972).
14. M. Hishida and T. Tsuji, Free convection heat transfer over a heated vertical plate, Preprint of 909th meeting of JSME, vol. 800–18, paper No. 210, 109–116 (1980).
15. G. de Vahl Davis and I. P. Jones, Natural convection in a square cavity. A comparison exercise, Jones I. P. and Thomson C. P. (eds). *Numerical solutions for a comparison problem on natural convection in an enclosed cavity*, AERE-R9955, HMSO, 1981.
16. H. Ozoe *et al.*, in preparation.
17. B. Staehle and E. Hähne, Overshooting and damped oscillations of transient natural convection in cavities, NC. 28, 287–292, Vol. 2, *Proc. Seventh International Heat Transfer Conference*, München, Hemisphere Publishing, Washington, DC (1982).
18. M. Hishida, Y. Nagano, T. Tsuzi and I. Kaneko, Turbulent boundary layer of free convection along a vertical plate., Preprint of 909th meeting of JSME, vol. No. 800–18, paper no. 211, 117–124 (1980), (In Japanese).
19. M. Miyamoto, H. Kajino, J. Kurima and I. Takanami, Development of turbulence characteristics in a vertical free convection boundary layer, NC34, 323–328, Vol. 2, *Proc. Seventh International Heat Transfer Conference*, München, Hemisphere Publishing, Washington, DC (1982).
20. W. Rodi, *Turbulence models and Their Application in Hydraulics*, International Association for Hydraulic Research, pp. 1–92, (1980).

**CALCUL NUMERIQUE DE LA CONVECTION NATURELLE LAMINAIRE OU
TURBULENTE D'EAU DANS UN CANAL RECTANGULAIRE AVEC DES PAROIS
OPPOSEES VERTICALES A TEMPERATURES DIFFERENTES**

Résumé—La convection naturelle est calculée par des méthodes de différences finies utilisant un modèle laminaire pour des enceintes 2×1 et 1×1 , Ra , variant entre 10^6 et 10^9 , des nombres $Pr = 5,12$ et $9,17$, et un modèle turbulent $k-\varepsilon$ pour une enceinte carrée avec Ra entre 10^{10} et 10^{11} et $Pr = 6,7$. Les nombres de Nusselt moyens s'accordent bien avec l'équation de Churchill pour les valeurs expérimentales ou calculées. Le profil de vitesse calculé le long de la paroi est en accord acceptable avec les valeurs expérimentales antérieures, excepté pour la fine couche limite sur la partie basse de la paroi où apparaît la nécessité d'un maillage plus fin qu'il n'est possible. On opère un test de sensibilité pour les constantes du modèle $k-\varepsilon$. Le profil de vitesse à mi-hauteur et le nombre de Nusselt moyen sont en meilleur accord avec les résultats expérimentaux lorsque le nombre de Prandtl turbulent est multiplié par quatre et la constante C_1 est diminuée de 10%. Un modèle turbulent plus fin et un maillage plus réduit apparaissent nécessaires, particulièrement aux grands Ra .

**NUMERISCHE BERECHNUNG DER LAMINAREN UND TURBULENTEN NATÜRLICHEN
KONVEKTION VON WASSER IN RECHTECKIGEN KANÄLEN**

Zusammenfassung—Es wurde die natürliche Konvektion mit einer Finite-Differenzen-Methode unter Anwendung eines laminaren Modells für 2 (Breite) $\times 1$ und 1×1 Querschnitte bei Ra von 10^6 bis 10^9 und $Pr = 5,12$ und $9,17$, sowie eines $k-\varepsilon$ Turbulenz-Modells für quadratische Querschnitte bei Ra von 10^{10} bis 10^{11} und $Pr = 6,7$ berechnet. Die mittlere Nusselt-Zahl stimmt mit der Korrelationsgleichung von Churchill für experimentelle und berechnete Werte gut überein. Das berechnete Geschwindigkeitsprofil entlang der beheizten Wand ist in annehmbarer Übereinstimmung mit früheren experimentellen Werten, außer in der dünnen Grenzschicht entlang des unteren Teils der Wand, wo eine engere Gitterweite, als bei der Berechnung möglich, erforderlich scheint. Ein detaillierter Sensitivitäts-Test für die Konstanten des $k-\varepsilon$ Modells wurde ebenfalls durchgeführt. Das Geschwindigkeitsprofil in mittlerer Höhe und die mittlere Nusselt-Zahl waren in noch besserer Übereinstimmung mit den experimentellen Ergebnissen, wenn die turbulente Prandtl-Zahl auf vier anstieg und die Konstante C_1 um 10% abnahm. Ein verfeinertes Turbulenz-Modell und eine engere Gitterunterteilung erscheint wünschenswert, insbesondere für große Ra -Zahlen.

**ЧИСЛЕННЫЙ РАСЧЕТ ЛАМИНАРНОЙ И ТУРБУЛЕНТНОЙ ЕСТЕСТВЕННОЙ
КОНВЕКЦИИ В ВОДЕ В ПРЯМОУГОЛЬНЫХ КАНАЛАХ С ИЗОТЕРМИЧЕСКИ
НАГРЕВАЕМЫМИ И ОХЛАЖДАЕМЫМИ ПРОТИВОПОЛОЖНЫМИ
ВЕРТИКАЛЬНЫМИ СТЕНКАМИ**

Аннотация—Рассчитывается конечно-разностными методами на ламинарной модели естественная конвекция в полостях с размерами 2 (ширина) $\times 1$ и 1×1 при значениях чисел Ra от 10^6 до 10^9 и $Pr = 5,12$ и $9,17$, а с помощью $k-\varepsilon$ модели турбулентности — конвекция в квадратной полости при числах Ra от 10^{10} до 10^{11} и $Pr = 6,7$. Средние значения числа Нуссельта хорошо согласуются с экспериментальными и расчетными значениями, полученными из обобщенной зависимости Черчилля. Расчетный профиль скорости вдоль нагреваемой стенки удовлетворительно совпадает с ранее полученными экспериментальными значениями, за исключением пограничного слоя небольшой толщины вдоль основания стенки, для которой необходимо использовать сетку с более мелким шагом, что не удалось осуществить практически. Исследована также устойчивость постоянных модели $k-\varepsilon$. Профиль скорости в средней части полости и средние значения числа Нуссельта лучше совпадали с экспериментальными данными, когда турбулентное число Прандтля возрастало до 4, а значения константы C_1 снижались на 10%. Необходима более адекватная модель турбулентности и сетка с более мелким шагом, особенно при больших значениях числа Ra .